ONCOIMMUNOLOGY
2022, VOL. 11, NO. 1, e2116844 (14 pages)
https://doi.org/10.1080/2162402X.2022.2116844

Taylor & Francis
Taylor & Francis Group

ORIGINAL RESEARCH

OPEN ACCESS Check for updates

IRE1α overexpression in malignant cells limits tumor progression by inducing an anti-cancer immune response

Adriana Martinez-Turtos[a,b], Rachel Paul[a,b], Manuel Grima-Reyes[a,b], Hussein Issaoui[a,b], Adrien Krug[a,b], Rana Mhaidly[a,b], Jozef P. Bossowski[a,b], Johanna Chiche[a,b], Sandrine Marchetti[a,b], Els Verhoeyen[a,b,c], Eric Chevet[d,e], and Jean-Ehrland Ricci[a,b]

[a]C3M, INSERM, Université Côte d'Azur, Nice, France; [b]Equipe labellisée Ligue Contre le Cancer, Nice, France; [c]CIRIINSERM U1111, Université de Lyon, Lyon, France; [d]Inserm U1242, Université de Rennes, Rennes, France; [e]Centre de lutte contre le cancer Eugène Marquis, Rennes, France

ABSTRACT

IRE1α is one of the three ER transmembrane transducers of the Unfolded Protein Response (UPR) activated under endoplasmic reticulum (ER) stress. IRE1α activation has a dual role in cancer as it may be either pro- or anti-tumoral depending on the studied models. Here, we describe the discovery that exogenous expression of IRE1α, resulting in IRE1α auto-activation, did not affect cancer cell proliferation *in vitro* but resulted in a tumor-suppressive phenotype in syngeneic immunocompetent mice. We found that exogenous expression of IRE1α in murine colorectal and Lewis lung carcinoma cells impaired tumor growth when syngeneic tumor cells were subcutaneously implanted in immunocompetent mice but not in immunodeficient mice. Mechanistically, the *in vivo* tumor-suppressive effect of overexpressing IRE1α in tumor cells was associated with IRE1α RNAse activity driving both XBP1 mRNA splicing and regulated IRE1-dependent decay of RNA (RIDD). We showed that the tumor-suppressive phenotype upon IRE1α overexpression was characterized by the induction of apoptosis in tumor cells along with an enhanced adaptive anti-cancer immunosurveillance. Hence, our work indicates that IRE1α overexpression and/or activation in tumor cells can limit tumor growth in immunocompetent mice. This finding might point toward the need of adjusting the use of IRE1α inhibitors in cancer treatments based on the predominant outcome of the RNAse activity of IRE1α.

ARTICLE HISTORY
Received 29 March 2022
Revised 19 August 2022
Accepted 19 August 2022

KEYWORDS
Cancer; UPR; IRE1α; XBP1s; RIDD; anti-cancer immunosurveillance; apoptosis

Introduction

The intense research for treatments against non-communicable diseases including metabolic disorders and cancer is increasingly focused on nutritional interventions. Indeed, dietary regimens such as caloric restriction, fasting, low carbohydrate and ketogenic diets as well as low protein and amino acid-restricted diets have shown some benefit in controlling tumor development and progression in preclinical and clinical studies.[1,2] The underlying molecular mechanisms of nutritional regimens that slow down tumor growth or extend animal survival include: (i) reduction of the insulin-like growth factor-1 (IGF-1)-triggered signaling cascades such as the PI3K/Akt/mTOR pathway, (ii) activation of AMPK, (iii) induction of apoptosis, (iv) DNA damage, (v) oxidative stress and (vi) alterations in proteostasis with induction of endoplasmic reticulum (ER) stress in tumor cells.[3–5] We have previously reported the tumor-suppressive effect of an isocaloric diet partially reduced in protein (Low PROT diet) on several cancer mouse models. We demonstrated that the anti-cancer immunosurveillance induced by the Low PROT diet was not dependent on mTOR activation but mediated, at least in part, via an inositol-requiring enzyme 1α (IRE1α)-dependent signaling pathway in tumor cells.[6]

IRE1α is a transducer of the Unfolded Protein Response (UPR). The UPR is canonically activated upon accumulation of improperly folded proteins in the ER but also by disturbances in the lipidic composition of the ER membrane.[7,8] IRE1α is a type I transmembrane protein that exhibits both kinase and endoribonuclease activities in its cytosolic domain. The serine/threonine kinase activity of IRE1α is responsible for its auto-transphosphorylation upon ER stress-dependent IRE1α dimerization, which in turn leads to activation of the IRE1α RNAse activity. Most of the IRE1α signaling outputs have so far been linked to its RNAse activity, first through the non-conventional splicing of XBP1 mRNA, that yields the transcription factor XBP1s, and second through RNA degradation (also called Regulated IRE1 Dependent Decay, RIDD).[9] The interplay between XBP1s and RIDD is key to control cell survival and cell death decisions under ER stress. Beyond these catalytic activities, IRE1α was recently described to exhibit scaffold functions that were associated with cell migration,[10] calcium signaling and bioenergetics.[11]

Alteration of ER homeostasis is associated with most cancer hallmarks and the IRE1α signaling has been extensively studied in preclinical models of solid and hematological cancers. For instance, constitutive activation of the IRE1α-XBP1 signaling in triple negative breast cancer (TNBC) has been reported to play a pro-tumorigenic role in xenografts and genetically modified mouse models through increased cytokine secretion, modulation of cancer cell stemness-like properties, response to hypoxia, induction

CONTACT Jean-Ehrland Ricci ricci@unice.fr C3M, INSERM, Université Côte d'Azur, équipe 3, 151 route de St Antoine de Ginestière, Nice, France
Supplemental data for this article can be accessed online at https://doi.org/10.1080/2162402X.2022.2116844

of angiogenesis, stroma remodeling of the tumor microenvironment (TME), chemotherapy resistance, and tumor relapse *in vivo*.[12–15] In genetic mouse models of pancreatic ductal adenocarcinoma (PDAC), IRE1α has also been involved in acquisition of a more aggressive tumor phenotype with mesenchymal-like properties and higher tumor-initiating and metastatic potential.[16,17] The IRE1α-XBP1 axis has been shown to be pro-tumorigenic in colon carcinoma mouse models via cell stemness-related processes[18] and resistance to chemotherapy in immunodeficient animals.[19] Interestingly, opposite functions of the two IRE1α RNAse activity outputs have been suggested in human glioblastoma multiforme and recapitulated in xenograft mouse models of glioblastoma. In these studies, XBP1s was described as pro-tumorigenic and RIDD as anti-tumorigenic.[20] The tumor-suppressive role of IRE1α was also documented in hematological cancers such as diffuse large B-cell lymphoma (DLBCL), more specifically of the germinal center B-cell-like (GCB) subtype. Indeed, a defective IRE1α-XBP1 pathway via epigenetic silencing of IRE1α has been recognized as a hallmark of GCB-DLBCL. Therefore, exogenous expression of XBP1s in subcutaneous xenografts of GCB-DLBCL in mice was found to limit tumor growth.[21] In contrast, in other non-Hodgkin's lymphomas such as Burkitt's lymphoma, the IRE1α-XBP1 axis promoted tumor growth.[22] This dual role of IRE1α signaling in cancer has also been described in different innate as well as adaptive immune cell populations within the TME of several solid oncogenic malignancies.[23–27]

Hence, since IRE1α plays a dual role in tumor progression, either pro- or anti-tumoral, we sought to investigate the effect of activating the IRE1α pathway by exogenous expression of IRE1α in tumor cells implanted in immunocompetent mice. We found that overexpression of IRE1α was detrimental to subcutaneous tumor growth of colorectal and Lewis lung carcinomas. Tumors with IRE1α overexpression were characterized by a higher anti-cancer immunosurveillance and tumor cells undergoing apoptosis.

Results

Low protein diet-dependent tumor suppression correlates with IRE1α activation in tumors, higher anti-cancer immunosurveillance and increased synthesis of pro-inflammatory cytokines

To determine how the Low PROT diet-induced IRE1α activation was involved in immunosurveillance, immunocompetent BALB/c mice were fed an isocaloric control (CTR) or Low PROT diet for 7 days prior to subcutaneous (SC) engraftment of syngeneic colorectal carcinoma CT26 cells (Figure 1a). Tumor-bearing mice were kept under diet until sacrifice and tumors were analyzed 15 days post-tumor engraftment. Low PROT tumors were significantly smaller than CTR tumors when tumor volume was measured by caliper and tumors were weighed after resection (Figure 1b). As we previously described,[6] total IRE1 α was not modulated but XBP1s protein levels were higher in Low PROT tumors confirming the activation of the IRE1α pathway (Figure 1c). Immune cell profiling indicated that tumor-infiltrating lymphocytes (TILs), specifically $CD8^+$ T cells (Figure 1d), tumor-associated macrophages (TAMs) (Figure 1e) and intra-tumoral dendritic cells (DCs, figure 1f) were enriched in Low PROT tumors. Correlating with higher recruitment of cytotoxic T cells into the TME of Low PROT tumors, a significant increase in the surface expression levels of MHC-I (Major Histocompatibility Complex-I, specifically H2Kd) was detected on isolated tumor cells from mice fed a Low PROT diet (Figure 1g). Furthermore, enhanced anti-tumoral effector functions of T lymphocytes from tumor-bearing mice fed the Low PROT diet were also observed by *ex vivo* cytotoxicity assay (Figure 1h).

Since IRE1α was activated and H2Kd was differentially expressed in Low PROT tumor cells, the transcript levels of gene encoding members of the antigen processing and presenting machinery and pro-inflammatory factors were quantified in isolated tumor cells from tumor-bearing mice. Transcript levels of ERAP1 (Endoplasmic Reticulum Aminopeptidase 1), an ER-resident aminopeptidase that generates peptide fragments that can be presented by MHC-I, were higher in Low PROT tumor cells (Figure 1i). Likewise, TAP1 (Transporter 1, ATP Binding Cassette Subfamily B) which is a member of a transporter complex localized in the ER membrane that shuttles cytoplasmic peptides into the ER to be trimmed and loaded onto MHC-I was also upregulated in Low PROT tumor cells (Figure 1i). Pro-inflammatory factors including type I interferons, TNF-α and GM-CSF, chemo-attractants (CXCL10, CXCL11, CCL2), and the NK cell-activating cytokine IL-15 were upregulated under the Low PROT diet (Figure 1j). These findings indicate that the Low PROT diet regulates gene expression in malignant cells, which might endow them with the ability to express more pro-inflammatory soluble factors and to increase the antigen processing and presenting machinery that enhance tumor immunogenicity and therefore, the anti-cancer immunosurveillance.

IRE1α overexpression in CT26 cells leads to IRE1α self-activation driving XBP1 mRNA splicing and RIDD induction

To test whether the Low PROT diet-induced anti-cancer immunosurveillance could be linked specifically to IRE1α activation in tumor cells, we exogenously expressed IRE1α (OE) and genetically silenced IRE1α in CT26 cells (KO). Stable IRE1α overexpression was confirmed by its higher transcript levels as compared to WT and mock cells (Figure 2a). Higher expression of IRE1α in OE cells resulted in IRE1α auto-activation as judged by the increase in XBP1 mRNA splicing as compared to control cells in basal conditions. XBP1s induction in IRE1α-overexpressing cells was similar to that in WT and mock cells treated with tunicamycin, which is a general inducer of ER stress. This suggests that exogenous expression of IRE1α induces a strong splicing of XBP1 (Figure 2a). Protein levels of IRE1α and XBP1s in IRE1α-overexpressing cells were in accordance with their transcript levels (Figure 2b). IRE1α overexpression resulted in induction of its RNAse activity beyond XBP1 splicing since lower transcript levels of the RIDD targets, Blos1 and Col6a1 were detected (Figure 2c)

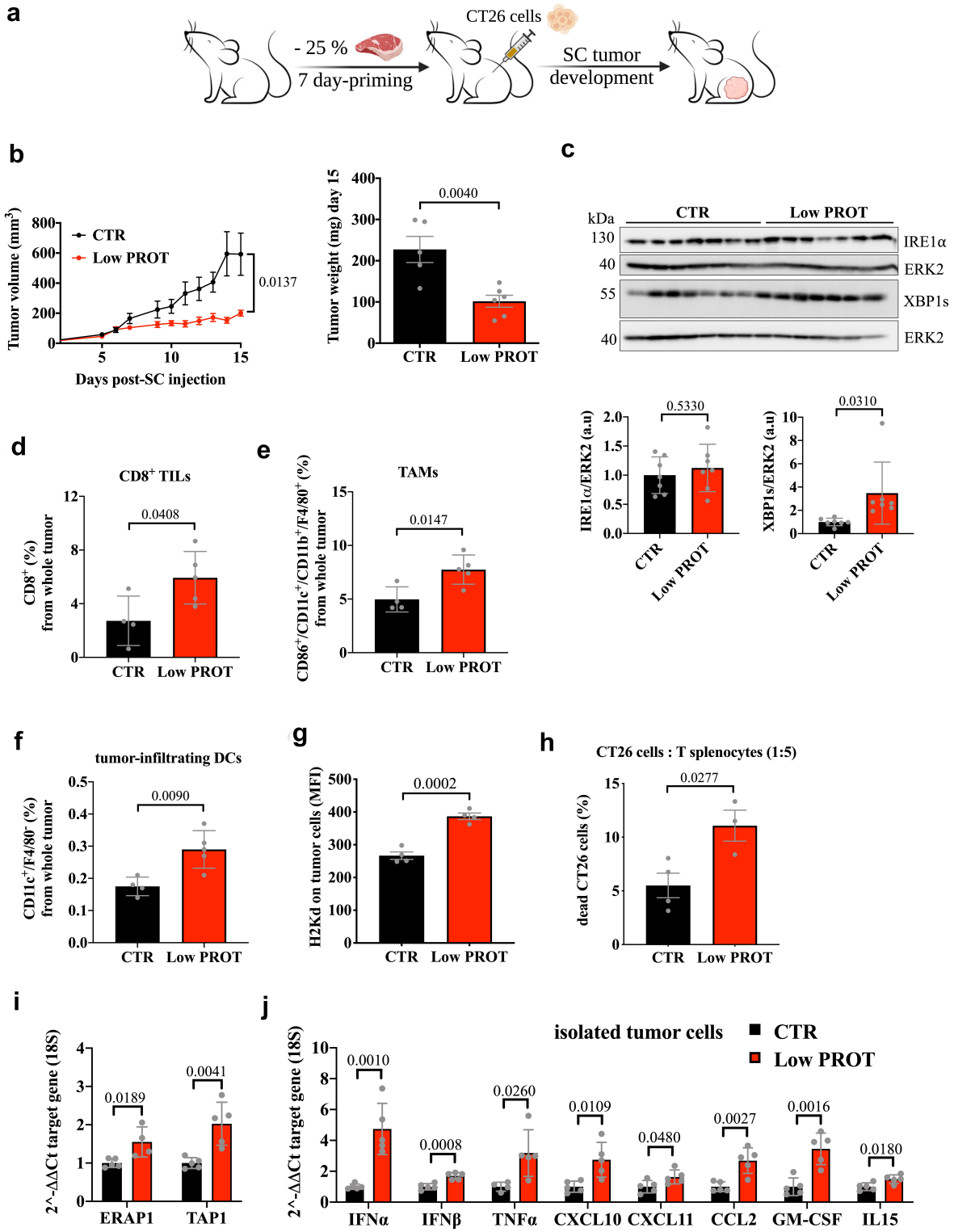

Figure 1. Low PROT diet limits tumor growth, activates the IRE1α pathway, increases the anti-cancer immunosurveillance and the synthesis of inflammatory genes. A. Immunocompetent BALB/c mice fed a control (CTR) or Low Protein (Low PROT) diet for 7 days were engrafted with syngeneic colorectal carcinoma CT26 cells. B. Subcutaneous (SC) tumor growth curve and tumor weight at endpoint (CTR, n = 5 and Low PROT, n = 6). C. Protein expression of IRE1α and XBP1s in whole tumors isolated from mice sacrificed at endpoint (15 days post-SC tumor cell injection, CTR, n = 7 and Low PROT, n = 7). ERK2 is used as a loading control. Quantification of IRE1alpha and XBP1s over ERK2 by densitometry analysis are presented below in arbitrary units (a.u.). D, E, F. Percentage of $CD8^+$ TILs, TAMs and intra-tumoral DCs from whole tumors presented in B, as quantified by flow cytometry (CTR, n = 4 and Low PROT, n = 5). G. Surface expression levels (MFI) of H2Kd determined by flow cytometry analysis on live and isolated tumor cells (CTR, n = 4 and Low PROT, n = 4) from mice sacrificed at endpoint. H. Percentage of dead CT26 cells co-cultured with $CD3^+$ T splenocytes isolated from tumor-bearing mice (from B) for *ex vivo* cytotoxicity assay (CTR, n = 4 and Low PROT, n = 3). I. Transcript levels in isolated tumor cells of proteins involved in the antigenic peptide shuttle into the ER and peptide loading onto MHC-I as quantified by RT-qPCR. J. Transcript levels in isolated tumor cells from B of type I and II interferons, cytokines, and chemokine ligands.Bars represent mean ± SD (or SEM for panel B) and each data point represents a biological replicate. Statistical differences were determined by two-tailed, unpaired Student's t-test. *In vivo* experiments are representative of several performed.

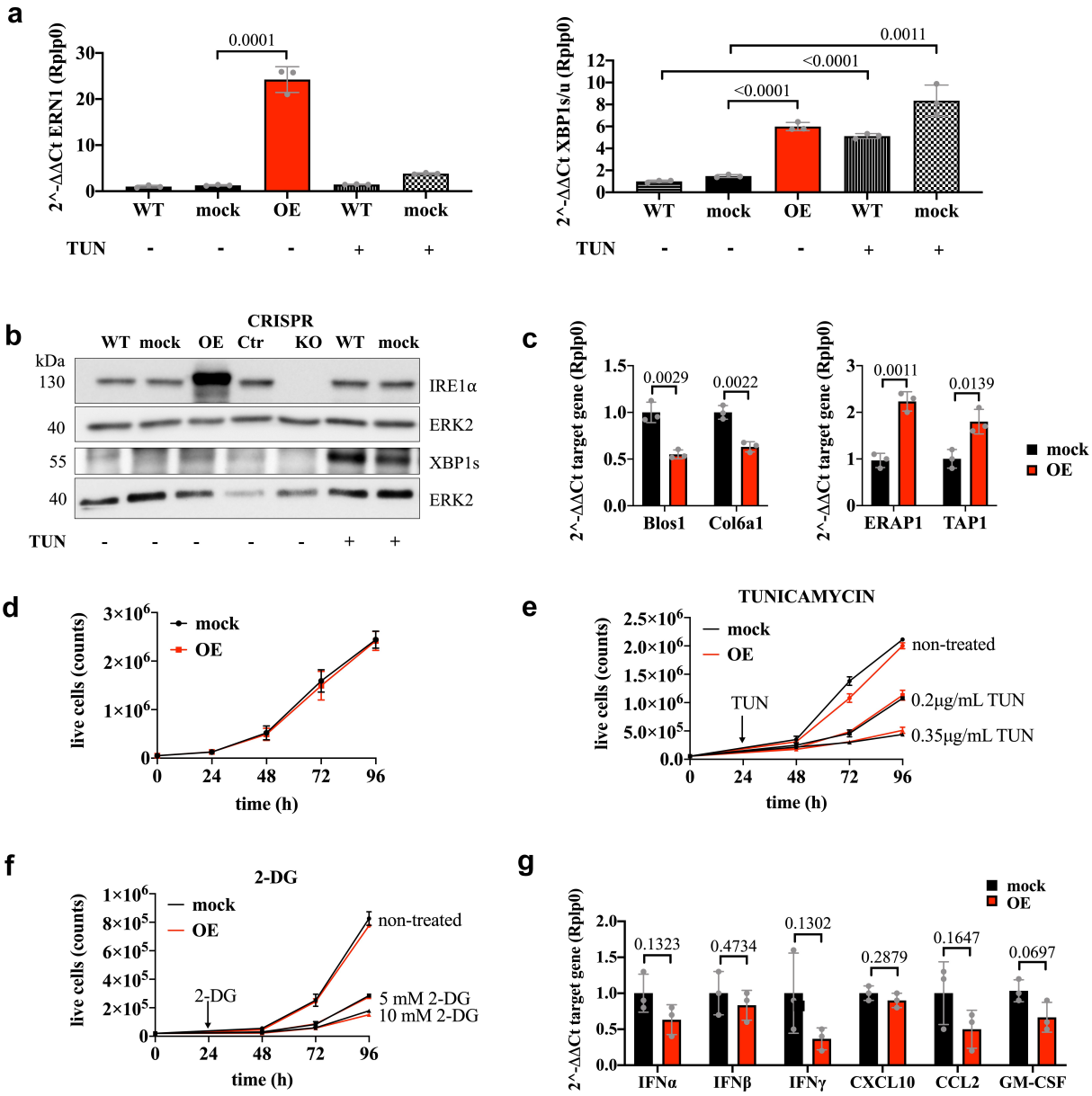

Figure 2. IRE1α-overexpressing CT26 cells display a functional IRE1α protein with an enhanced endoribonuclease activity. A. Transcript expression levels of ERN1 and XBP1s/u in WT, mock and IRE1α-overexpressing (OE) in basal conditions and under tunicamycin 1 μg/mL for 16 hours (presented as the average of technical triplicates of three independent experiment). B. Protein expression levels of IRE1α and XBP1s were determined by immunoblotting in WT, mock, OE, CRISPR Ctr, and KO CT26 cells in basal conditions and under tunicamycin 1 μg/mL for 16 hours (representation of one out of three independent experiments). ERK2 is used as a loading control. C. Transcript levels of RIDD targets (biological replicates of three independent experiments), ERAP1, and TAP1 (technical triplicates of a single experiment) in mock and OE CT26 cells were quantified by RT-qPCR. D. Cell growth of mock and IRE1α OE CT26 cells (biological replicates of three independent experiments). E. Cell growth of mock and OE CT26 cells when treated with the indicated doses of tunicamycin (biological triplicates of a single experiment). F. Cell growth of mock and OE CT26 cells when treated with the indicated doses of 2-DG (2-deoxyglucose, biological triplicates of a single experiment). G. Transcript level expression of type I and II interferons, ligands of chemokines and cytokines in mock and OE CT26 cells were quantified by RT-qPCR (technical triplicates of a single experiment). Bars and data points of the cell growth curves represent mean ± SD. Statistical differences were determined by two-tailed, unpaired Student's t-test.

indicating RIDD induction. ERAP1 and TAP1 transcripts which were upregulated in isolated tumor cells from Low PROT diet-fed mice (Figure 1i) also increased in IRE1α-overexpressing cells as compared to mock cells (Figure 2c). IRE1α-overexpressing CT26 cells displayed in vitro a proliferative capacity similar to that of control cells (Figure 2d). Even though cell growth of IRE1α-overexpressing cells decreased under treatment with tunicamycin (Figure 2e) or 2-deoxyglucose (figure 2f), two ER stress inducers, we could not observe a significant difference with control cells, indicating that IRE1α overexpression is not sensitizing CT26 cells growing *in vitro* to stress-induced cytostatic or cytotoxic effects.

Interestingly, transcript levels of several cytokines that were upregulated in Low PROT tumor cells did not increase in IRE1α-overexpressing cells (Figure 2g). This finding suggests that IRE1α overexpression in *in vitro* cultured CT26 cells did not have an impact on cytokine production contrary to what had been reported in triple negative breast cancer cells that display constitutive IRE1α RNAse activity with enhanced XBP1 splicing.[12] Hence, exogenous expression of IRE1α in CT26 drives XBP1 mRNA splicing and RIDD induction with no changes in cell

proliferation *in vitro* even under ER stress induced by various pharmacological treatments.

IRE1α-overexpressing tumors display a limited tumor growth, tumor cell apoptosis and higher immune cell infiltration

To evaluate the impact of IRE1α activity on tumor growth and immunogenicity, IRE1α-overexpressing (OE) CT26 cells were subcutaneously engrafted in syngeneic immunocompetent BALB/c mice. IRE1α overexpression yielded a drastic reduction in tumor size when compared to control tumors (Figure 3a). Importantly, this effect was also observed in a subcutaneous syngeneic mouse model of Lewis lung carcinoma since IRE1α-overexpressing LLC1 cells yielded smaller tumors as compared to control tumors in C57BL/6 mice (Figure 3b). Prior to *in vivo* engraftment, IRE1α-overexpressing LLC1 cells were generated and validated *in vitro* showing higher transcript levels of IRE1α along with a significant increase of XBP1 mRNA splicing (Fig. S1A). IRE1α overexpression in LLC1 cells did not change their proliferative capacity *in vitro* (Fig. S1B).

In BALB/c mice bearing tumors, we verified that protein levels of IRE1α and XBP1s were increased in isolated tumor cells from IRE1α-overexpressing (OE) CT26 tumors (Figure 3c) and that no significant changes in protein levels of other UPR members, namely, ATF4 and CHOP were observed between mock and OE CT26 tumor cells (Figure 3c). Analysis of isolated OE CT26 tumor cells from the mice presented in Figure 3a, confirmed transcriptional upregulation of IRE1α and induction of its full RNAse activity as judged by the upregulation of XBP1s and downregulation of RIDD targets (Figure 3d). The extent of RIDD induction beyond XBP1 splicing suggested that a pro-death outcome of the IRE1α-RIDD axis could underlie tumor growth limitation upon exogenous expression of IRE1α. Indeed, a close characterization of the tumor cells isolated at endpoint from Figure 3a, indicated that OE CT26 tumor cells undergo apoptosis *in vivo* as judged by increased cleavage of PARP (Figure 3e), a canonical caspase substrate, and increased DEVDase activity (figure 3f). Intra-tumoral immune profiling of OE CT26 tumor-bearing mice revealed higher infiltration of immune cells (Figure 3g). Among them, TILs, specifically $CD3^+$ T cells, cytotoxic $CD8^+$ T cells and total $CD4^+$ T cells (without discrimination between helper and regulatory $CD4^+$ T cells, Figure 3h) were higher in OE CT26 tumors. In addition, tumor-infiltrating NK cells (Figure 3i) and resident TAMs (Figure 3j) were higher in OE tumors. $CD11c^+$ resident TAMs were shown to express higher levels of activation markers like MHC-II and CD86 (Figure 3j). Surface expression levels of MHC-I (specifically H2Kd) and CD47 were upregulated and downregulated, respectively, on tumor cells (Figure 3k). This correlated with the upregulation of H2Kd seen in Low PROT tumor cells (Figure 1g). Surface expression of another MHC-I variant of the same haplotype (H2Ld) and the MHC class I-like molecule (H60) did not change in OE cells (Figure 3k). Importantly, isolated $CD3^+$ T splenocytes from OE tumor-bearing mice displayed higher cytotoxicity when co-cultured *in vitro* with CT26 cells (Figure 3l), indicating a specific adaptive anti-cancer immune response in these mice. Hence, IRE1α overexpression in CT26 and LLC1 tumors is associated with limited tumor progression in immunocompetent mice, via the induction of tumor cell death and a higher immune cell infiltrate.

IRE1α knockout in CT26 favors in vivo *tumor growth*

To test whether the impairment of tumor growth associated with exogenous expression of IRE1α can be reverted by knocking out IRE1α, CRISPR/Cas9 control (CRISPR Ctr) and IRE1α knockout (KO) CT26 cells were generated. As expected, IRE1α KO CT26 cells did not express IRE1α protein (Figure 2b), did not show splicing of XBP1 (Figure 4a) and did not affect *in vitro* cell proliferation (Figure 4b). Then, IRE1α KO CT26 cells were subcutaneously implanted into immunocompetent BALB/c mice. It is important to note that, as detailed in the Materials and Methods section, IRE1α was genetically invalidated in CT26 cells by transient transfection to avoid any immunogenicity that might be related to the exogenous expression of the Cas9 nuclease. Knockout of IRE1α enhanced tumor growth as compared to control cells (Figure 4c). In addition, KO tumors displayed lower infiltration of $CD8^+$ T cells (Figure 4d) and lower expression of the activation marker MHC-II on $CD11c^+$ resident TAMs (Figure 4e), inversely correlating with the enhanced immune cell infiltration and expression of activation markers on TAMs observed in OE CT26 tumors (Figure 3h,j). In this line, surface expression of MHC-I (H2Kd and H2Ld) (figure 4f) was downregulated on KO tumor cells while CD47 and H60 expression was unaltered (figure 4f). These findings indicate that exogenous expression of IRE1α in CT26 tumor cells impairs tumor growth as demonstrated by the opposite tumor phenotype driven by IRE1α genetic invalidation.

IRE1α overexpression-associated tumor suppression is partially dependent on cytotoxic T cells

To document the impact of IRE1α overexpression on cell death and the adaptive immune response, we engrafted OE CT26 cells into immunodeficient Nude mice that lacked functional T and B cells. The engraftment of IRE1α overexpressing CT26 cells revealed a trend but no significant impairment of the tumor growth as judged by the tumor weight at endpoint (Figure 5a). We confirmed that IRE1α transcript levels were significantly higher in isolated OE CT26 tumor cells. This, indeed, correlated with induction of a full RNAse activity based on transcriptional upregulation of XBP1s and downregulation of RIDD targets (Figure 5b). OE CT26 tumor cells isolated from tumor-bearing Nude mice displayed higher caspase activity (Figure 5c). This result recapitulates the enhanced caspase activity observed in OE CT26 tumor-bearing immunocompetent mice (figure 3f), even if it did not result in a significant reduction in tumor weight. Immune cell profiling showed higher infiltration of NK cells (Figure 5d) and of resident TAMs expressing MHC-II in OE tumors as compared to control tumors (Figure 5e). Although cell surface expression of H2Kd and CD47 did not change, H60, an activating ligand

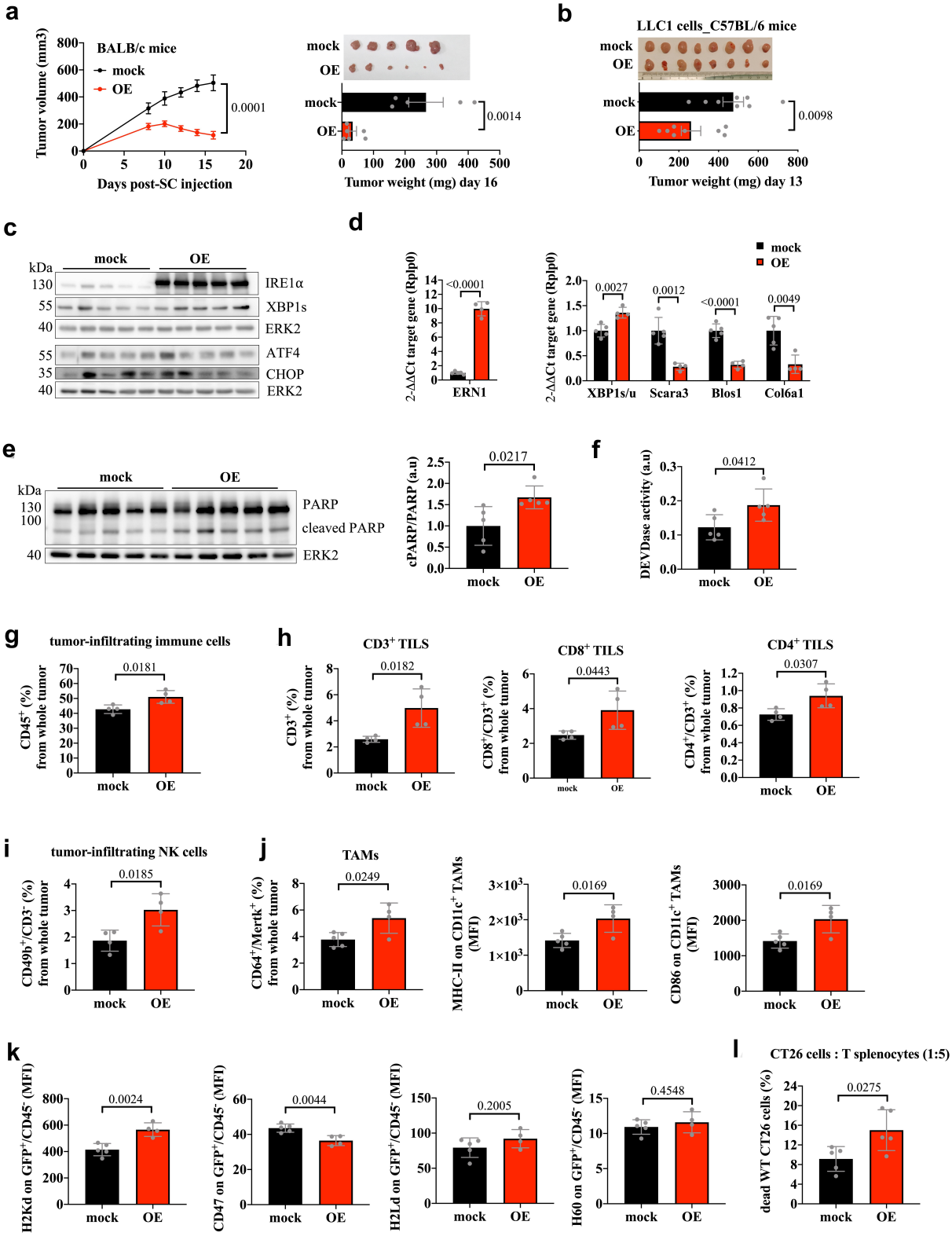

Figure 3. IRE1α overexpression in CT26 tumor cells limits tumor growth in immunocompetent syngeneic mice. A. Subcutaneous (SC) tumor growth curve (left) and tumor weight at endpoint (day 16 post-SC injection, right) of immunocompetent BALB/c mice engrafted with mock and IRE1α-overexpressing (OE) CT26 cells (CTR n=5, OE, n=6). B. Tumor weight at endpoint (day 13 post-SC injection) of immunocompetent C57BL/6 mice subcutaneously engrafted with mock and IRE1α-overexpressing (OE) LLC1 cells (n = 8 per group). C. Protein expression levels of IRE1α, XBP1s, and other UPR components (CHOP, ATF4) in isolated tumor cells from CT26 tumor-bearing mice sacrificed at endpoint (day 16 post-SC tumor cell injection, CTR = 5 and OE = 5). ERK2 is used as a loading control. D. Transcript expression levels of IRE1α, XBP1s/u and RIDD targets (Scara3, Blos1, Col6a1) in isolated tumor cells from CT26 tumor-bearing mice sacrificed at endpoint were quantified by RT-qPCR (CTR = 5 and OE = 4). E. Protein expression levels of PARP and cleaved PARP in isolated tumor cells from CT26 tumor-bearing mice sacrificed at endpoint (CTR = 5 and OE = 5). ERK2 is used as a loading control. To the right, quantification of cleaved over total PARP by densitometry analysis. F. Caspase (DEVDase) activity in isolated tumor cells from CT26 tumor-bearing mice sacrificed at endpoint (CTR = 5 and OE = 5). G. Percentage of $CD45^+$ cells from CT26 whole tumors presented in A. H. Percentage of $CD3^+$ TILs, $CD8^+$ TILs, and $CD4^+$ TILs from whole CT26 tumors presented in A. I. Percentage of tumor-infiltrating NK cells from whole CT26 tumors presented in A. J. Percentage of resident TAMs from whole CT26 tumors presented in A. and surface expression levels (MFI) of MHC-II and CD86 on $CD11c^+$ resident TAMs. K. Surface expression levels (MFI) of

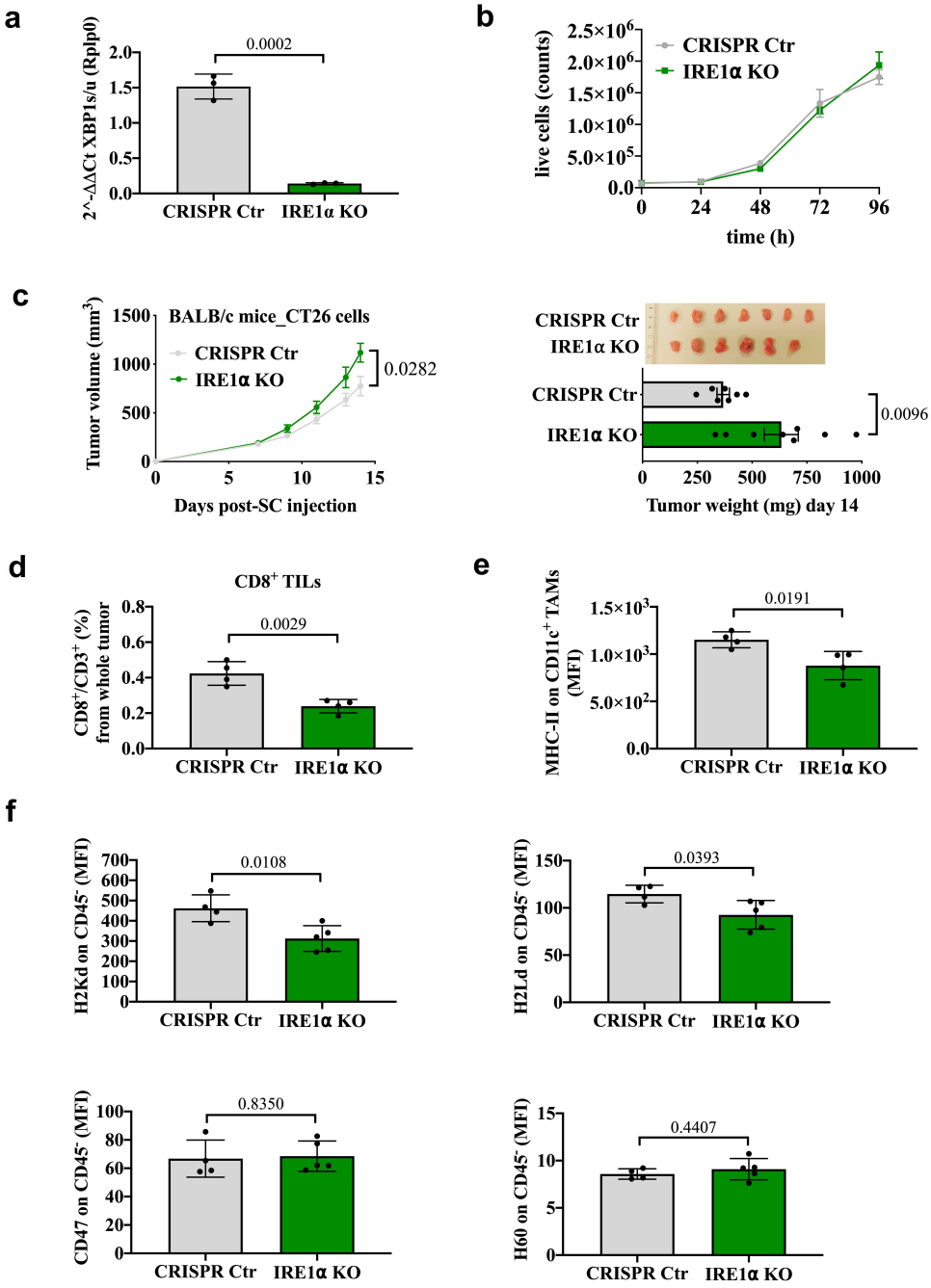

Figure 4. IRE1α knockout in CT26 tumor cells enhances tumor growth in immunocompetent mice. A. Transcript expression levels of XBP1s/u in CRISPR Control (Ctr) and IRE1α-KO CT26 cells in basal conditions in vitro. B. Cell growth of CRISPR Control (Ctr) and IRE1α-KO CT26 cells. C. Subcutaneous (SC) tumor growth curve and tumor weight at endpoint (day 14 post-SC injection) of immunocompetent BALB/c mice engrafted with CRISPR/Cas9 control (CRISPR Ctr) (n = 7) and IRE1α knockout (KO) (n = 8) CT26 cells. D. Percentage of $CD8^+$ TILs from whole CT26 tumors presented in C. E. Surface expression levels (MFI) of MHC-II on CD11c+ resident TAMs from whole CT26 tumors. F. Surface expression levels (MFI) of immune markers on live CRISPR Ctr and KO CT26 tumor cells ($CD45^-/DAPI^-$) (CRISPR Ctr = 4 and IRE1α KO = 4/5). From D to F, tumors were resected from mice sacrificed at endpoint and immune cell populations were quantified by flow cytometry. Bars represent mean ± SD (or SEM for panel C), and each data point represents biological replicates. Statistical differences were determined by two-tailed, unpaired Student's t-test.

of NK cells, was upregulated on OE tumor cells (figure 5f). These results suggest that IRE1α overexpression in tumor cells induces cell death *in vivo* and higher recruitment of immune cells into the TME. However, IRE1α OE-associated

immune markers on live mock and OE CT26 tumor cells ($GFP^+/CD45^-/DAPI^-$) presented in A. From G to K, tumors were resected from mice sacrificed at endpoint and immune cell populations were quantified by flow cytometry (CTR = 4/5 and OE = 4). L. $CD3^+$ T splenocytes were isolated from mice bearing mock or OE-CT26 tumors at endpoint and incubated with WT CT26 for 4 hours (ratio: 5 T cells for 1 CT26 cell). The ability of T cells to kill tumoral cells was determined by DAPI staining and measured by flow cytometry (CTR = 5 and OE = 5). Bars represent mean ± SD (or SEM for panel A and B), and each data point represents biological replicates. Statistical differences were determined by two-tailed, unpaired Student's t-test. *In vivo* results are representative of at least two experiments performed.

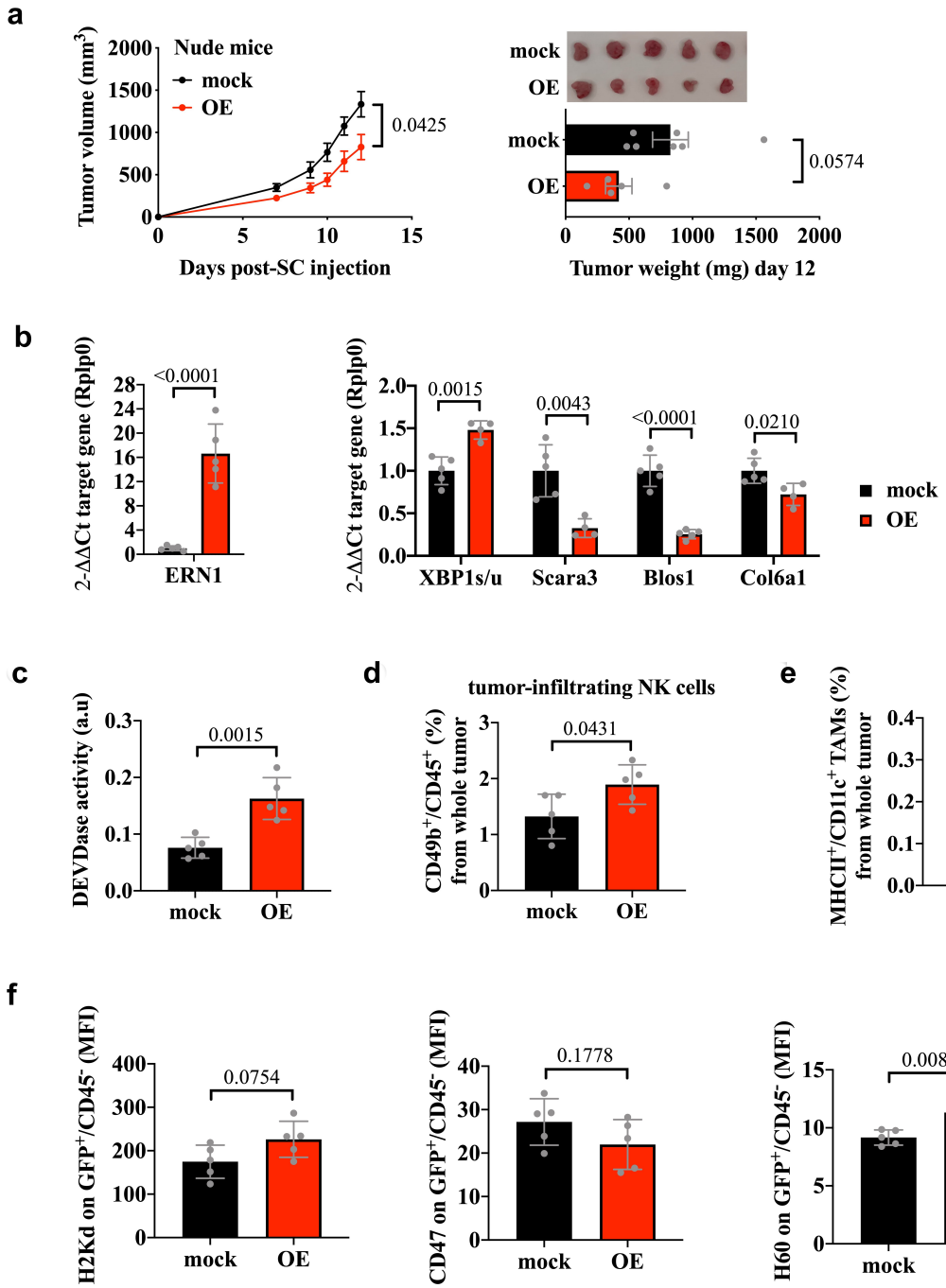

Figure 5. IRE1α overexpression in CT26 tumor cells limits tumor growth and is partially dependent on T cells. A. Subcutaneous (SC) tumor growth curve and tumor weight at endpoint (day 12 post-SC injection) of immunodeficient Nude mice engrafted with mock (n = 7) and IRE1α-overexpressing (OE) CT26 cells (n = 5). B. Transcript expression levels of IRE1α, XBP1s/u and RIDD targets (Scara3, Blos1, Col6a1) in isolated tumor cells from tumor-bearing mice sacrificed at endpoint were quantified by RT-qPCR (CTR = 5 and OE = 4/5). C. Caspase (DEVDase) activity in isolated tumor cells from tumor-bearing mice sacrificed at endpoint (CTR = 5 and OE = 5). D, E. Percentage of resident TAMs and tumor-infiltrating NK cells from whole tumors resected from mice at endpoint. F. Surface expression levels (MFI) of immune markers on live mock and OE tumor cells ($GFP^+/CD45^-/DAPI^-$) of mice sacrificed at endpoint (CTR = 4/5 and OE = 5). From D to F, quantification by flow cytometry. Bars represent mean ± SD (or SEM for panel A) and each data point represents biological replicates. Statistical differences were determined by two-tailed, unpaired Student's t-test.

cell death did not significantly reduce tumor growth (Figure 5a) in the absence of functional adaptive immune cells, even if the intra-tumoral infiltration of other immune cells (such as NK cells and TAMs) was higher in OE tumors (Figure 5d,e).

Altogether, IRE1α activation in tumor cells via exogenous expression of IRE1α yields a less aggressive tumor phenotype and associates with apoptosis in tumor cells growing *in vivo* and a stronger anti-cancer immunosurveillance partially dependent on T cells (Figure 6).

Discussion

We have shown that exogenous expression of IRE1α in tumor cells results in an anti-tumoral phenotype in immunocompetent (Figure 3) but not in immunodeficient mice (Figure 5). This

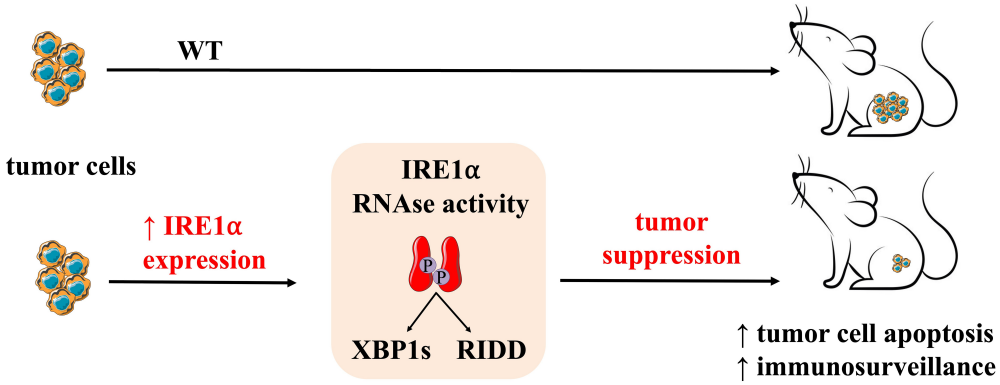

Figure 6. The RNAse activity of IRE1α in tumor cells limits tumor growth. An enhanced RNAse activity of IRE1α by its exogenous expression in tumor cells leads to XBP1 splicing and RIDD induction in malignant cells and limits subcutaneous tumor growth of colorectal and Lewis lung carcinoma. The tumor-suppressive effect of exogenous expression of IRE1α in malignant cells associates with induction of apoptosis in tumor cells and a higher anti-cancer immunosurveillance in immunocompetent mice.

finding correlates with the tumor growth limitation observed under the Low PROT diet (Figure 1). The tumor-suppressive functions of IRE1α correlated, beyond XPB1 splicing, with RIDD induction in tumor cells and with an increase in tumor cell death and higher immune cell infiltrate (Figures 3 and 6). Indeed, this anti-tumoral phenotype was further supported by the pro-tumoral effect of IRE1α genetic invalidation in CT26 tumor cells (Figure 4). We demonstrated that the anti-tumoral phenotype associated with IRE1α exogenous expression in tumors partially depended on cytotoxic T cells (Figure 5). This result is different from the anti-cancer immunosurveillance induced by the Low PROT diet, as the latter was entirely dependent on $CD8^+$ T cells.[6] These findings indicate that the anti-cancer immune response enhanced by the nutritional approach (the Low PROT diet) is different from that induced by the genetic approach (IRE1α overexpression), probably due to the activation of different molecular mechanisms and/or different systemic aspects (such as microbiota modulation). Also, the fact that the low PROT diet was provided prior to inoculation of tumor cells could impact seeding and subsequent tumor growth.

Beyond the information that the nature of IRE1α RNAse activities (XBP1s vs RIDD) is a key factor in regulating tumor growth-associated outputs, our data also suggest that the expression level of IRE1α on its own could also be a factor to consider. It is plausible that exogenous expression of IRE1α could alter IRE1α scaffolding functions and the subsequent biological outputs. In many cases, the pro-tumoral role of IRE1α is associated with XBP1 mRNA splicing, which when coupled with certain oncogenic drivers copes with the inherent cytotoxicity of rapidly proliferating tissues. In parallel, the expression of XBP1s supports tumor cells in the stressful TME deprived of nutrients and oxygen. Indeed, XBP1s has been shown to confer tumor cells the ability of initiating tumor growth and of responding to hypoxia in cooperation with HIF-1α.[13] Hence, XBP1s and its tumor-protective effects might be the result of adaptive ER stress mechanisms induced to support the competitive tumor cell growth.

The tumor-protective role of the IRE1α-XBP1 axis has been positively associated with the expression of c-Myc in TNBC,[14] PDAC,[16] and in high c-Myc human B cell lymphomas and N-Myc-driven human neuroblastoma.[22] In this regard, depending on the oncogenic driver, signaling pathways supporting the tumor proliferative capacity and anabolic metabolism vary among different cell and cancer types. Therefore, tumors expressing high levels of c-Myc and XBP1s such as TNBC could benefit from the inhibition of this signaling axis. Altogether, the oncogenic drivers, the type of cancer, the immunocompetence of cancer animal models and subcutaneous or orthotopic tumors may account for the dual role of the IRE1α pathway in cancer. Considering the transformed cell lines used in our study, genomic characterization of colorectal carcinoma CT26 cells has shown a homozygous mutation of Kras at $G^{12}D$ and no mutation but a high expression of Myc, p53, Mdm2, HIF1-α and Nras.[28] In Lewis lung carcinoma LLC1 cells, a heterozygous Kras mutation is present at $G^{12}C$ with not description of alterations in Myc.[29] This might account for the tumor-suppressive role of IRE1α overexpression in these cells since the oncogenic driver is Kras and not c-Myc, and the IRE1α pathway is oriented toward RIDD in parallel with XBP1splicing.

Exogenous expression of IRE1α in our model resulted in a full induction of its endoribonuclease activity with no changes in the *in vitro* cell proliferative capacity even upon extra ER and nutritional stresses (Figure 2). Despite the robustness of IRE1α-overexpressing cells in *in vitro* settings, *in vivo* implanted cells within the restrictive TME displayed an impaired growth. We can speculate that the strong induction of RIDD beyond XBP1 splicing in tumor cells growing *in vivo* might be responsible for driving terminal UPR and subsequently apoptosis in IRE1α-overexpressing cells. This hypothesis is supported by a study suggesting that XBP1 splicing and RIDD induction, when uncoupled, are associated with tumor protection and suppression, respectively.[20] Indeed, tumor cells undergoing apoptosis were a common feature of the immunocompetent and the immunodeficient cancer mouse models in our study. Certainly, most studies define IRE1α activation based on XBP1 splicing but selective and massive degradation of some mRNAs and miRNAs could also dictate tumor growth progression.[20]

Irrespective of tumor cell apoptosis, an enhanced anti-cancer immune response was seen in IRE1α-overexpressing tumors. The less aggressive tumor phenotype might be a combination of

intrinsic apoptosis induced by toxic IRE1α exogenous expression in tumor cells growing *in vivo* and an anti-cancer immune response elicited by the immunogenic tumor cell death. Likewise, a potent anti-cancer immunosurveillance elicited by plasma membrane-bound and soluble factors secreted by tumor cells at early stages during tumor progression cannot be ruled out. Indeed, MHC-I was upregulated in tumor cells from tumor-bearing immunocompetent mice in parallel with a downregulation of CD47, the 'don't eat me' signal that inhibits the phagocytic activity of macrophages. In addition, in immunodeficient mice, H60, an activating ligand of NK cell receptors was found upregulated. We can hypothesize that in the absence of functional T cells in Nude mice, cytotoxic NK cells played a major role in controlling tumor growth.[30] Therefore, modulation of immune markers on tumor cells overexpressing IRE1α and consequent activation of immune cells is a plausible mechanism underlying tumor growth limitation.

In this regard, the IRE1 pathway has been reported to regulate MHC-I either by promoting MHC-I expression via XBP1s or by decreasing MHC-I expression via RIDD.[31–33] This model was described for a specific subtype of DCs that displays constitutive activation of the IRE1 pathway.[34] Therefore, regulation by the IRE1 pathway of MHC-I expression as well as the mechanisms of antigen processing and presentation in tumor cells is plausible in our study.

We consistently recapitulated tumor-suppressive phenotypes under a Low PROT diet and upon exogenous expression of IRE1α in tumor cells. However, distinctive features of each model (nutritional or genetic) were observed beyond the degree of dependence on the anti-cancer adaptive immune response. For instance, the Low PROT diet modulated the synthesis of several pro-inflammatory factors in tumor cells while IRE1α-overexpression in CT26 cells did not change the transcript levels of these cytokines and chemo-attractants, which might correlate with a RIDD characteristic. Features shared between the nutritional and the genetic model include higher expression of genes coding for members of the antigen processing and presenting machinery and indeed, upregulation of MHC-I on tumor cells.

Beyond the Low PROT diet as an anti-cancer nutritional intervention and the IRE1α pathway functioning as a tumor-suppressive signaling cascade in tumoral cells, this study indicates that identifying the most predominant output of IRE1α RNAse activity is an important parameter before designing anti-cancer therapies targeting this pathway. As suggested by a study in glioblastoma multiforme, analysis of XBP1s and RIDD signatures in tumors could be informative of the type of anti-cancer drugs that can better control tumor progression.[20] While tumors with IRE1α-XBP1 arm activation with low RIDD induction might be sensitive to pharmacological inhibition of IRE1α with selective inhibitors, tumors with predominant IRE1α-RIDD axis activation with low XBP1 splicing might instead be controlled by pro-apoptotic inducers. Pro-apoptotic drugs could synergize with the pro-death cellular outcome mediated by massive RIDD induction.[20] Overall, this work reinforces the idea that a thorough characterization of the IRE1α pathway beyond XBP1 splicing in tumor cells could be a critical criterion to consider before selecting the most appropriate anti-cancer therapies.

Materials and methods

Mice

All animal experiments were performed according to the guidelines of the Institutional Animal Care and Use Committee and the regional ethics committee (approval references PEA-503 and PEA-673). All experiments used age-matched five-week-old female littermates. WT syngeneic BALB/c and C57BL/6 mice as well as Nude mice were obtained from ENVIGO and housed in our animal facility (C3M-Nice, France). When specified, mice were fed isocaloric diets purchased from ENVIGO: either the Control (CTR: TD.130931) or the Low Protein diet (Low PROT −25%: TD.130933). The caloric composition of these diets (% of energy provided by carbohydrate: protein: fat content) was the following: CTR – (70.9%: 19.5%: 9.6%) and Low PROT −25% – (73.7%: 14.9%: 11.5%), see.[6] Mice were fed the specified diets for 7 days prior to subcutaneous engraftment of tumor cells. WT syngeneic BALB/c and Nude mice were subcutaneously engrafted with 0.75×10^6 CT26 cells while C57BL/6 mice were subcutaneously engrafted with 0.5×10^6 LLC1. After subcutaneous engraftment of CT26 and LLC1 cells, mice were inspected every two days for tumor development. Tumor growth was monitored by caliper measurement following the equation (width^2 x length)/2. Animals were sacrificed when a tumor reached at least 1000 mm^3.

Cell lines and cell culture conditions

CT26 cells were obtained from the ATCC (#CRL-2638) and cultured in RPMI-1640 medium (Gibco) supplemented with 10% fetal bovine serum (FBS), 1% penicillin-streptomycin (5000 U/mL) (Gibco), and 1% sodium pyruvate (Gibco). LL/2 (LLC1) cells were obtained from the ECACC (#90020104) and cultured in DMEM (Gibco) supplemented with 10% FBS. All cell lines were mycoplasma free. CT26 and LLC1 cells were seeded and cultured for 48 h prior to cell engraftment into mice and for validation of IRE1α expression and activity by RT-qPCR. CT26 and LLC1 cells were treated with tunicamycin at 1 μg/mL for 16 h. For cell growth experiments, CT26 cells were seeded, and 24 h later tunicamycin (Sigma-Aldrich) or 2-deoxyglucose (Sigma-Aldrich) were added at the indicated concentrations for a total cell culture of 96 h. All experiments were performed in duplicates or triplicates. All cell lines were incubated at 37°C in a 5% CO^2 atmosphere.

Generation of mock and IRE1α-overexpressing cells

A lentiviral vector coding for human IRE1α (hERN1) and GFP under the control of the SFFV promoter was designed (pLV[Exp]-SFFV>SalI/hERN1[NM_001433.5](ns)}:T2A/SalI:EGFP) and purchased from VectorBuilder (VB201207-1387mct). This lentiviral vector was used to generate the control vector that only expresses GFP. In summary, the lentiviral vector was designed to contain SalI restriction sites upstream of the insert (hERN1) and downstream of the T2A sequence. Enzymatic digestion with SalI and re-ligation at 16°C for 16 h yielded the control plasmid coding for GFP under control of the

SFFV promoter. For generating transduced cells, self-inactivating viruses were generated by transient transfection of 293 T cells (ATCC, #CRL-1573) and titered as described previously.[35] Briefly, using the classical calcium phosphate method, the envelope plasmid VSV-G (3 µg) was co-transfected with 8.6 µg of Gag-Pol packaging plasmid (psPAX2, Adgene, #12260) and 8.6 µg of the empty lentiviral vector coding for GFP or the lentiviral vector coding for hERN1α (VB201207-1387mct). Eighteen hours after transfection, the medium was replaced by Opti-MEM supplemented with 1% HEPES (Invitrogen). Viral supernatants were harvested 48 h after transfection and filtered with a 0.45 µm filter. The vectors were concentrated at low speed by overnight centrifugation of the viral supernatants at 3000 g and 4°C. Viral particles were titered in CT26 and LLC1 cells. CT26 and LLC1 cells were transduced with viruses at a multiplicity of infection (MOI) equivalent to 1. Cells were seeded overnight ($8x10^4$ cells) in 6-well culture plates prior to virus addition to the cell culture media. Cells were kept in the same media up to 48 h before medium refreshment and cell expansion. Transduced cells were sorted (SONY sorter SH800, Sony Biotechnology) based on stable GFP expression, resulting in >95% purity. Exogenous expression of hIRE1α was verified by RT-qPCR and immunoblotting.

Generation of CRISPR/Cas9 cells

For the generation of stable CT26 cells with invalidated IRE1α, cells were transfected with 3 µg of CRISPR-Cas9-expressing knockout plasmids (control, sc-418922 and IRE1α, sc-429758 from Santa Cruz) using the jetPEI DNA transfection reagent (PolyPlus Transfection, #POL101-10 N) as described by the manufacturer. The knockout plasmid was a mixture of three plasmids, each carrying a different guide RNA specific to the target gene and to the Cas- and GFP-coding regions. Transient GFP positive cells were selected by sorting (SONY sorter SH800, Sony Biotechnology) 24 h after transfection. IRE1α knockout (KO) was verified by immunoblotting.

Analysis of quantitative reverse transcription PCR (RT-qPCR)

For *in vitro* cultured cells, cells seeded for 48 h were detached with trypsin-EDTA 0.25% (Gibco) and collected. Cell pellets were lysed in tryzol prior to RNA extraction with chloroform. Reverse transcription was performed using the Omniscript RT Kit (Qiagen, #205113). Quantitative-PCR was performed with Power SYBR Green PCR master mix (Applied Biosystems, Life Technologies, # 4367659) using the Step One real-time PCR system (Applied Biosystems) following the manufacturers' instructions. For whole tumors, a piece of the frozen tissue was cut and mechanically disrupted in tryzol using a Pre-cellys 24 tissue homogenizer (Bertin Instruments) (3 x 30s, 6,500 x *g*). For the analysis of tumor cells from tumor-bearing mice, tumors were enzymatically digested with the Tumor Dissociation Kit for mice (Miltenyi Biotec, #130-096-730) yielding a single tumor cell suspension. Tumor cells were magnetically isolated using the Tumor Cell Isolation kit for mice (Miltenyi Biotec, 130–110-187) following the manufacturers' instructions. In brief, dissociated tumors were incubated with a depletion cocktail for 15 min and after magnetic isolation using an AutoMACS Pro Separator (Miltenyi Biotec), the negative fractions containing tumor cells and the positive fractions containing stromal cells were frozen either as a dry pellet or in 10% DMSO-containing FBS.

The following primers for mouse sequences were used for SYBR Green qPCR:

Gene	Primer sequences (forward 5′-3′ / reverse 5′-3′)
ERN1	AGAGAAGCAGCAGACTTTGTC GTTTTGGTGTCGTACATGGTGA
XBP1u	GAGTCCGCAGCACTCAGACT GTGTCAGAGTCCATGGGAAGA
XBP1s	GCTGAGTCCGCAGCAGGTG GTGTCAGAGTCCATGGGAAGA
Scara3	TGACAGGGATGTACTGTGTGT TGCAAAGATAGGTTCTTCTGGC
Blos1	CAAGGAGCTGCAGGAGAAGA GCCTGGTTGAAGTTCTCCAC
Col6a1	TGCTCAACATGAAGCAGACC TTGAGGGAGAAAGCTCTGGA
IFNα	AGCAGATCCAGAAGGCTCAA GGAGGGTTGTATTCCAAGCA
IFNβ	GCAGCTGAATGGAAAGATCA TGGCAAAGGCAGTGTAACTC
IFNγ	TCAAGTGGCATAGATGTGGAAGAA TGGCTCTGCAGGATTTTCATG
TNFα	CCCTCACACTCAGATCATCTTCT GCTACGACGTGGGCTACAG
CXCL10	CCAAGTGCTGCCGTCATTTTC GGCTCGCAGGGATGATTTCAA
CXCL11	GGCTTCCTTATGTTCAAACAGGG GCCGTTACTCGGGTAAATTACA
CCL2	TTAAAAACCTGGATCGGAACCAA GCATTAGCTTCAGATTTACGGGT
GM-CSF	TCGTCTCTAACGAGTTCTCCTT CGTAGACCCTGCTCGAATATCT
IL15	ACATCCATCTCGTGCTACTTGT GCCTCTGTTTTAGGGAGACCT
Rn18S	GTAACCCGTTGAACCCCATT CCATCCAATCGGTAGTAGCG
Rplp0	AGATTCGGGATATGCTGTTGGC TCGGGTCCTAGACCAGTGTTC

ERN1 primers were designed to recognize mouse and human sequences. Transcript levels of XBP1s were normalized over the trancript levels of XBP1u. The housekeeping genes Rn18S and Rplp0 were used as control for RNA quality and normalization. All analyses were performed in technical triplicates and the SYBR Green melting curve analysis was performed to control product quality and specificity.

Western blot analysis

For whole tumors, the frozen tissue was homogenized using a stainless-steel tissue grinder (1292, BioSpec Products). Tumor powder was lysed in a protease inhibitor-containing Laemmli or RIPA buffer using a Pre-cellys 24 tissue homogenizer (Bertin Instruments) (3 x 30s, 6500 x *g*). Magnetically isolated tumor cells (Tumor Cell Isolation kit for mice (Miltenyi Biotec, 130–110-187) were lysed in a protease inhibitor-containing RIPA buffer. Protein lyses were quantified and standardized (Pierce BCA protein assay kit, Thermo Scientific, #23225), and immunoblots were developed using the Amersham ECL Prime Western Blotting Detection Reagent (Cytiva, #RPN2236) and visualized with ImageQuant LAS 4000 (GE Healthcare, Life Science). Densitometry analyses were performed with the Multi Gauge v3 software. For *in vitro* cultured cells, Laemmli buffer for lysis and the XBP1s antibody (Biolegend #658802) were used while the XBP1 antibody (Santa Cruz #8015) was used for whole tumors lysed in Laemmli buffer and isolated tumor cells lysed in RIPA buffer. The following antibodies were used for immunoblotting:

Antibody	Source	Identifier
Rabbit monoclonal anti-IRE1α	Cell Signaling	3294; RRID:AB_823545
Mouse monoclonal anti-XBP1	Santa Cruz	sc-8015; RRID:AB_628449
Mouse monoclonal anti-XBP1s	Biolegend	658802, RRID:AB_2562960
Mouse monoclonal anti-CHOP	Cell Signaling	2895; RRID:AB_2089254
Rabbit monoclonal anti-ATF4	Cell Signaling	11815; RRID:AB_2616025
Rabbit polyclonal anti-PARP	Cell Signaling	9542, RRID:AB_2160739
Mouse monoclonal anti-ERK2	Santa Cruz	sc-1647; RRID:AB_627547

Flow cytometry analysis

CT26 tumors were dissociated using the Tumor Dissociation Kit for mice (Miltenyi Biotec, #130-096-730) yielding a single-cell suspension. Stained samples were analyzed with a MACSQuant Analyzer 10 (Miltenyi Biotec). The following fluorochrome-conjugated anti-mouse antibodies were used for flow cytometry and isolation of $CD3^+$ splenocytes:

Antibody	Source	Identifier (cat #, RRID)
APC-eFluor 780 anti-CD45.2	eBioscience, Thermo Fisher Scientific	47–0454-80, RRID: AB_1272211
PE anti-H-2Kd	BD Biosciences	553566, RRID: AB_394924
PE anti-H-2Ld/H-2 Db	BioLegend	114507, RRID: AB_313588
PE-Cyanine7 anti-CD274 (PD-L1, B7-H1)	eBioscience, Thermo Fisher Scientific	25–5982-82, RRID: AB_2573509
APC anti-H60a	REAfinity, Miltenyi Biotec	130–108-847, RRID: AB_2651975
PE-Vio770 anti-CD47	REAfinity, Miltenyi Biotec	130–103-105, RRID: AB_2659751
APC anti-CD3	BioLegend	Cat# 100236, RRID: AB_2561456
PE-Vio770 anti-CD8a	REAfinity, Miltenyi Biotec	130–119-123, RRID: AB_2733250
V450 anti-CD4	BD Biosciences	560468, RRID: AB_1645271
CD152 Antibody, anti-mouse, PE	Miltenyi Biotec	130–102-570, RRID: AB_2655252
PE-Vio770 anti-CD49b	Miltenyi Biotec	130–105-402, RRID: AB_2660461
Brilliant Violet 42 anti-CD64 (FcgammaRI)	BioLegend	139309, RRID: AB_2562694
PE anti-MERTK (Mer)	Biolegend	151505, RRID: AB_2617036
Alexa Fluor 647 anti-I-A/I-E	Biolegend	107617, RRID: AB_493526
PE-Cyanine7 anti-CD86 (B7-2)	eBioscience, Thermo Fisher Scientific	25–0862-82, RRID: AB_2573372
eFluor 450 anti-F4/80	eBioscience, Thermo Fisher Scientific	48–4801-82, RRID: AB_1548747
PE/Cy7 anti-CD11c	BD Biosciences	558079, RRID: AB_647251
FITC anti-CD11b	BD Biosciences	553310, RRID: AB_394774
PE anti-CD11c	BD Bioscience	557401, RRID: AB_396684
PE anti-annexin V	Miltenyi Biotec	130–118-499
FITC anti-CD19	Miltenyi Biotec	130–102-494, RRID: AB_2661108
FITC anti-CD45R (B220)	REAfinity, Miltenyi Biotec	130–110-708, RRID: AB_2658274)
FITC anti-CD49b	Miltenyi Biotec	130–102-258, RRID: AB_2660456
FITC anti-Ter-119	REAfinity, BD Biosciences	130–112-719, RRID: AB_2654114

Intra-tumoral infiltration of immune cell populations was calculated as a percentage of the whole tumor. Tumor-infiltrating lymphocytes (TILs) were defined as followed: $CD3^+$ TILs ($CD3^+/CD45^+$), $CD8^+$ TILs ($CD8^+/CD3^+$), and $CD4^+$ TILs ($CD4^+/CD3^+$). Infiltrating NK cells were defined as $CD49b^+/CD3^-/CD45^+$. Tumor assoiated macrophages (TAMs) were defined as $CD86^+/CD11c^+/CD11b^+/F4/80^+/CD45^+$ in CTR and Low PROT tumors, while resident TMAs were defined as $CD64^+/Mertk^+/CD45^+$ cells in mock and over-expressed tumors. Mock and IRE1α-overexpressing tumor cells were defined as $GFP^+/CD45^-$ while CRISPR/Cas control and IRE1α knockout tumor cells were defined as $CD45^-$ cells.

Cytotoxicity assay

Spleens were manually smashed and filtered through a 40 μm strainer to obtain a single-cell suspension of splenocytes. $CD3^+$ cells were depleted by magnetic isolation using an autoMACS Pro Separator (Miltenyi Biotec) after staining with FITC-conjugated antibodies against CD19 (Miltenyi, #130-102-494), CD45R (Miltenyi, #130-110-708), CD49b (Miltenyi, #130-102-258), CD11b (BD Bioscience, #553310) and Ter-119 (Miltenyi, #130-112-719). The resulting purified cells were co-cultured with CT26 cells at a ratio of 5:1 in the presence of IL-2 (1 ng/mL, Miltenyi Biotec #130-094-055) for 4 h at 37°C. Cell death of CT26 cells was monitored by $DAPI^+$ staining and flow cytometry (MACSQuant Analyzer 10, Miltenyi Biotec).

Cell death measurement

Cell death was analyzed either by DEVDase activity or 4',6-diamidino-2-phenylindole staining (DAPI, Sigma-Aldrich #D9542). To measure apoptosis in isolated tumor cells, the activity of DEVDases was assayed as described previously[36] with some modifications. Briefly, cells were lysed in a lysis buffer (50 mM HEPES [pH 7.4], 150 mM NaCl, 20 mM EDTA, 0.2% NP40, 2 μg/mL aprotinin, 1 mM PMSF, and 10 μg/mL leupeptin). Protein lysates were quantified and standardized (Pierce BCA protein assay kit, Thermo Scientific, #23225) and loaded into a black 96-well plate (CellStar) in the presence of 0.2 mmol/L of the caspase-3 substrate Ac-DEVD-AMC (Enzo LifeScience, ALX-260-031-M005) diluted in the lysis buffer containing 10 mmol/L DTT. Caspase activity was determined either in the absence or presence of 1 mmol/L of the caspase inhibitor Ac-DEVD- CHO (Enzo LifeScience, ALX-260-030-M001) using a fluoroscan recording the emission fluorescence at 460 nm (Fluoroskan Ascent, Thermo Scientific). The specific DEVDase activity was calculated as the change in fluorescence per minute.

Statistical analysis

Graphs and statistical tests were generated using Prism v.8 (GraphPad software, Inc.). Differences in calculated means between groups were assessed by two-tailed, unpaired Student's t tests. A p-value less than 0.05 was considered significant.

Acknowledgments

We gratefully acknowledge the Animal facility at the Centre Méditerranéen de Médecine Moléculaire (C3M). We thank Camila Rubio-Patiño for her intellectual support.

Disclosure statement

No potential conflict of interest was reported by the author(s).

Funding

This work was supported by la Ligue Nationale Contre le Cancer "Equipe Labellisée", la Fondation ARC pour la Recherche sur le Cancer, by Institut National du Cancer (INCa PLBIO) and le Cancéropôle PACA and l'Agence Nationale de la Recherche (LABEX SIGNALIFE ANR-11-LABX-0028-01). This project received funding from the European Union's Horizon 2020 research and innovation program under the Marie Skłodowska-Curie grant agreement No. 766214 (Meta-Can). A. M.-T. was supported by la Fondation pour la Recherche Médicale (FRM) grant No. FDT202012010714.

Author contributions

A.M.-T. performed most of the research described herein and was assisted by R.P.-B., M.G.-R., H.I., R.M., E.V., J.P.B., and A.K. E.V., S.M., J.C., and M.G.-R. provided intellectual input and experimental designs. E. C. provided invaluable reagents and inputs. J.-E.R. designed the research, secured funding and wrote the manuscript.

References

1. Levesque S, Pol JG, Ferrere G, Galluzzi L, Zitvogel L, Kroemer G. Trial watch: dietary interventions for cancer therapy. Oncoimmunology. 2019;8(7):1591878. doi:10.1080/2162402X.2019.1591878.
2. Kanarek N, Petrova B, Sabatini DM. Dietary modifications for enhanced cancer therapy. Nature. 2020;579(7800):507–517. doi:10.1038/s41586-020-2124-0.
3. Tajan M, Vousden KH. Dietary approaches to cancer therapy. Cancer Cell. 2020;37:767–785. doi:10.1016/j.ccell.2020.04.005.
4. Sahu N, Dela Cruz D, Gao M, Sandoval W, Haverty PM, Liu J, Stephan J-P, Haley B, Classon M, Hatzivassiliou G, et al. Proline starvation induces unresolved ER stress and hinders mTORC1-Dependent tumorigenesis. Cell Metab. 2016;24(5):753–761. doi:10.1016/j.cmet.2016.08.008.
5. Meynet O, Ricci JE. Caloric restriction and cancer: molecular mechanisms and clinical implications. Trends Mol Med. 2014;20:419–427. doi:10.1016/j.molmed.2014.05.001.
6. Rubio-Patino C, Bossowski JP, De Donatis GM, Mondragon L, Villa E, Aira LE, Chiche J, Mhaidly R, Lebeaupin C, Marchetti S, et al. Low-protein diet induces IRE1alpha-Dependent anticancer immunosurveillance. Cell Metab. 2018;27(828–842):e827. doi:10.1016/j.cmet.2018.02.009.
7. Halbleib K, Pesek K, Covino R, Hofbauer HF, Wunnicke D, Hanelt I, Hummer G, Ernst R. Activation of the unfolded protein response by lipid bilayer stress. Mol Cell. 2017;67(673–684):e678. doi:10.1016/j.molcel.2017.06.012.
8. Covino R, Hummer G, Ernst R. Integrated functions of membrane property sensors and a hidden side of the unfolded protein response. Mol Cell. 2018;71(3):458–467. doi:10.1016/j.molcel.2018.07.019.
9. Hetz C, Axten JM, Patterson JB. Pharmacological targeting of the unfolded protein response for disease intervention. Nat Chem Biol. 2019;15(8):764–775. doi:10.1038/s41589-019-0326-2.
10. Urra H, Henriquez DR, Canovas J, Villarroel-Campos D, Carreras-Sureda A, Pulgar E, Molina E, Hazari YM, Limia CM, Alvarez-Rojas S, et al. IRE1α governs cytoskeleton remodelling and cell migration through a direct interaction with filamin A. Nat Cell Biol. 2018;20:942–953. doi:10.1038/s41556-018-0141-0.
11. Carreras-Sureda A, Jana F, Urra H, Durand S, Mortenson DE, Sagredo A, Bustos G, Hazari Y, Ramos-Fernández E, Sassano ML, et al. Non-canonical function of IRE1alpha determines mitochondria-associated endoplasmic reticulum composition to control calcium transfer and bioenergetics. Nat Cell Biol. 2019;21:755–767. doi:10.1038/s41556-019-0329-y.
12. Logue SE, McGrath EP, Cleary P, Greene S, Mnich K, Almanza A, Chevet E, Dwyer RM, Oommen A, Legembre P, et al. Inhibition of IRE1 RNase activity modulates the tumor cell secretome and enhances response to chemotherapy. Nat Commun. 2018;9(1):3267. doi:10.1038/s41467-018-05763-8.
13. Chen X, Iliopoulos D, Zhang Q, Tang Q, Greenblatt MB, Hatziapostolou M, Lim E, Tam WL, Ni M, Chen Y, et al. XBP1 promotes triple-negative breast cancer by controlling the HIF1alpha pathway. Nature. 2014;508:103–107. doi:10.1038/nature13119.
14. Zhao N, Cao J, Xu L, Tang Q, Dobrolecki LE, Lv X, Talukdar M, Lu Y, Wang X, Hu DZ, et al. Pharmacological targeting of MYC-regulated IRE1/XBP1 pathway suppresses MYC-driven breast cancer. J Clin Invest. 2018;128(4):1283–1299. doi:10.1172/JCI95873.
15. Harnoss JM, Le Thomas A, Reichelt M, Guttman O, Wu TD, Marsters SA, Shemorry A, Lawrence DA, Kan D, Segal E, et al. IRE1alpha disruption in triple-negative breast cancer cooperates with antiangiogenic therapy by reversing ER stress adaptation and remodeling the tumor microenvironment. Cancer Res. 2020;80:2368–2379. doi:10.1158/0008-5472.CAN-19-3108.
16. Genovese G, Carugo A, Tepper J, Robinson FS, Li L, Svelto M, Nezi L, Corti D, Minelli R, Pettazzoni P, et al. Synthetic vulnerabilities of mesenchymal subpopulations in pancreatic cancer. Nature. 2017;542(7641):362–366. doi:10.1038/nature21064.
17. Robinson CM, Talty A, Logue SE, Mnich K, Gorman AM, Samali A. An emerging role for the unfolded protein response in pancreatic cancer. Cancers (Basel). 2021;14:13. doi:10.3390/cancers14010013.
18. Li XX, Zhang HS, Xu YM, Zhang RJ, Chen Y, Fan L, Qin Y-Q, Liu Y, Li M, Fang J, et al. Knockdown of IRE1alpha inhibits colonic tumorigenesis through decreasing beta-catenin and IRE1alpha targeting suppresses colon cancer cells. Oncogene. 2017;36:6738–6746. doi:10.1038/onc.2017.284.
19. Gao Q, Li XX, Xu YM, Zhang JZ, Rong SD, Qin YQ, Fang J. IRE1alpha-targeting downregulates ABC transporters and overcomes drug resistance of colon cancer cells. Cancer Lett. 2020;476:67–74. doi:10.1016/j.canlet.2020.02.007.
20. Lhomond S, Avril T, Dejeans N, Voutetakis K, Doultsinos D, McMahon M, Pineau R, Obacz J, Papadodima O, Jouan F, et al. Dual IRE1 RNase functions dictate glioblastoma development. EMBO Mol Med. 2018;10(3): e7929. doi:10.15252/emmm.201707929.
21. Bujisic B, De Gassart A, Tallant R, Demaria O, Zaffalon L, Chelbi S, Gilliet M, Bertoni F, Martinon F. Impairment of both IRE1 expression and XBP1 activation is a hallmark of GCB DLBCL and contributes to tumor growth. Blood. 2017;129(17):2420–2428. doi:10.1182/blood-2016-09-741348.
22. Xie H, Tang CH, Song JH, Mancuso A, Del Valle JR, Cao J, Xiang Y, Dang CV, Lan R, Sanchez DJ, et al. IRE1alpha RNase-dependent lipid homeostasis promotes survival in Myc-transformed cancers. J Clin Invest. 2018;128:1300–1316. doi:10.1172/JCI95864.
23. Rubio-Patino C, Bossowski JP, Chevet E, Ricci JE. Reshaping the immune tumor microenvironment through IRE1 signaling. Trends Mol Med. 2018;24:607–614. doi:10.1016/j.molmed.2018.05.005.
24. Cubillos-Ruiz JR, Silberman PC, Rutkowski MR, Chopra S, Perales-Puchalt A, Song M, Zhang S, Bettigole S, Gupta D, Holcomb K, et al. ER stress sensor XBP1 controls anti-tumor

immunity by disrupting dendritic cell homeostasis. Cell. 2015;161 (7):1527–1538. doi:10.1016/j.cell.2015.05.025.
25. Ma X, Bi E, Lu Y, Su P, Huang C, Liu L, Wang Q, Yang M, Kalady MF, Qian J, et al. Cholesterol induces CD8(+) T cell exhaustion in the tumor microenvironment. Cell Metab. 2019;30 (143–156):e145. doi:10.1016/j.cmet.2019.04.002.
26. Song M, Sandoval TA, Chae CS, Chopra S, Tan C, Rutkowski MR, Raundhal M, Chaurio RA, Payne KK, Konrad C, et al. IRE1alpha-XBP1 controls T cell function in ovarian cancer by regulating mitochondrial activity. Nature. 2018;562:423–428. doi:10.1038/s41586-018-0597-x.
27. Dong H, Adams NM, Xu Y, Cao J, Allan DSJ, Carlyle JR, Chen X, Sun JC, Glimcher LH. The IRE1 endoplasmic reticulum stress sensor activates natural killer cell immunity in part by regulating c-Myc. Nat Immunol. 2019;20(7):865–878. doi:10.1038/s41590-019-0388-z.
28. Castle JC, Loewer M, Boegel S, de Graaf J, Bender C, Tadmor AD, Boisguerin V, Bukur T, Sorn P, Paret C, et al. Immunomic, genomic and transcriptomic characterization of CT26 colorectal carcinoma. BMC Genomics. 2014;15(1):190. doi:10.1186/1471-2164-15-190.
29. Agalioti T, Giannou AD, Krontira AC, Kanellakis NI, Kati D, Vreka M, Pepe M, Spella M, Lilis I, Zazara DE, et al. Mutant KRAS promotes malignant pleural effusion formation. Nat Commun. 2017;8(1):15205. doi:10.1038/ncomms15205.
30. Obiedat A, Seidel E, Mahameed M, Berhani O, Tsukerman P, Voutetakis K, Chatziioannou A, Mcmahon M, Avril T, Chevet E, et al. Transcription of the NKG2D ligand MICA is suppressed by the IRE1/XBP1 pathway of the unfolded protein response through the regulation of E2F1. FASEB J. 2019;33:3481–3495. doi:10.1096/fj.201801350RR.
31. Osorio F, Tavernier SJ, Hoffmann E, Saeys Y, Martens L, Vetters J, Delrue I, De Rycke R, Parthoens E, et al. The unfolded-protein-response sensor IRE-1alpha regulates the function of CD8alpha+ dendritic cells. Nat Immunol. 2014;15:248–257. doi:10.1038/ni.2808. PMID: 24441789.
32. Medel B, Costoya C, Fernandez D, Pereda C, Lladser A, Sauma D, Pacheco R, Iwawaki T, Salazar-Onfray F, Osorio F, et al. IRE1alpha activation in bone marrow-derived dendritic cells modulates innate recognition of melanoma cells and favors CD8(+) T cell priming. Front Immunol. 2018;9:3050. doi:10.3389/fimmu.2018.03050. PMID: 30687308.
33. Guttman O, Le Thomas A, Marsters S, Lawrence DA, Gutgesell L, Zuazo-Gaztelu I, et al. Antigen-derived peptides engage the ER stress sensor IRE1alpha to curb dendritic cell cross-presentation. J Cell Biol. 2022;221.
34. Osorio F, Lambrecht BN, Janssens S. Antigen presentation unfolded: identifying convergence points between the UPR and antigen presentation pathways. Curr Opin Immunol. 2018;52:100–107. doi:10.1016/j.coi.2018.04.020.
35. Frecha C, Fusil F, Cosset FL, Verhoeyen E. In vivo gene delivery into hCD34+ cells in a humanized mouse model. Methods Mol Biol. 2011;737:367–390.
36. Villa E, Proics E, Rubio-Patino C, Obba S, Zunino B, Bossowski JP, Rozier RM, Chiche J, Mondragón L, Riley JS, et al. Parkin-Independent mitophagy controls chemotherapeutic response in cancer cells. Cell Rep. 2017;20(12):2846–2859. doi:10.1016/j.celrep.2017.08.087.